THE JOURNAL OF PHYSICAL CHEMISTRY LETTERS
A JOURNAL OF THE AMERICAN CHEMICAL SOCIETY

pubs.acs.org/JPCL Letter

Controlling Vibronic Coupling in Chlorophyll Proteins: The Effects of Excitonic Delocalization and Vibrational Localization

Galina Grechishnikova, Jacob H. Wat, Nicolas de Cordoba, Ethan Miyake, Amala Phadkule, Amit Srivastava, Sergei Savikhin, Lyudmila Slipchenko, Libai Huang, and Mike Reppert*

Cite This: J. Phys. Chem. Lett. 2024, 15, 9456−9465 Read Online

ACCESS | Metrics & More | Article Recommendations | Supporting Information

ABSTRACT: Vibrational−electronic (vibronic) coupling plays a critical role in excitation energy transfer in molecular aggregates and pigment−protein complexes (PPCs). But the interplay between excitonic delocalization and vibronic interactions is complex, often leaving even qualitative questions as to what conceptual framework (e.g., Redfield versus Förster theory) should be used to interpret experimental results. To shed light on this issue, we report here on the interplay between excitonic delocalization and vibronic coupling in site-directed mutants of the water-soluble chlorophyll protein (WSCP), as reflected in 77 K fluorescence spectra. Experimentally, we find that in PPCs where excitonic delocalization is disrupted (either by mutagenesis or heterodimer formation), the relative intensity of the vibrational sideband (VSB) in fluorescence spectra is suppressed by up to 37% compared to that of the native protein. Numerical simulations reveal that this effect results from the localization of high-frequency vibrations in the coupled system; while excitonic delocalization suppresses the purely electronic transition due to H-aggregate-like dipole−dipole interference, high-frequency vibrations are unaffected, leading to a relative enhancement of the VSB. By comparing VSB intensities of PPCs both in the presence and absence of excitonic delocalization, we extract a set of "local" Huang−Rhys (HR) factors for Chl *a* in WSCP. More generally, our results suggest a significant role for geometric effects in controlling energy-transfer rates (which depend sensitively on absorption/fluorescence line shapes) in molecular aggregates and PPCs.

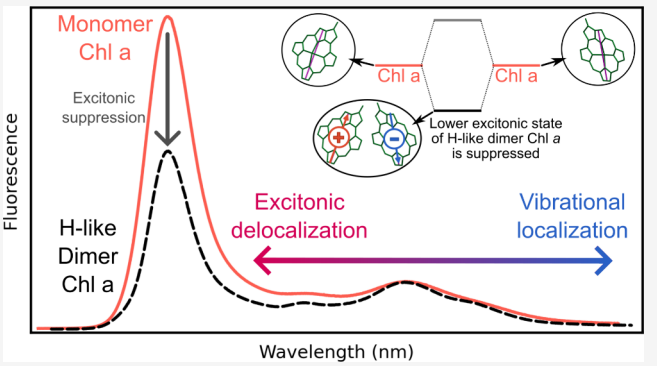

Vibrational−electronic (vibronic) interactions have long been known to play a role in photosynthetic light harvesting.[1−11] In the incoherent limit of Förster resonance energy transfer (FRET), vibrations shape the absorption−fluorescence overlap integrals that govern energy transfer from one pigment to the next.[12] In the opposite extreme, vibrational structure determines the spectral densities that govern energy relaxation between coherent excitonic states.[1] Discrete vibrations, typically localized to the pigment and distinct from the broader phonon bands of the protein, can even promote coherent effects through vibronic resonance.[13,14]

Yet this very diversity of roles makes it difficult to identify the precise function of vibronic interactions in any given system.[15−19] Most chlorophyll proteins (CPs) operate in an "intermediate coupling" regime where the overall strength of vibronic interactions, electronic site-to-site coupling between pigment transitions, and static disorder in local transition frequencies (site energies) all have comparable magnitudes, on the order of tens to hundreds of wavenumbers (cm^{-1}).[20] In this intermediate regime, the role of vibrational coupling is complex. Vibrational interactions could either enhance delocalization through vibronic resonance or suppress it by acting as a thermal bath.[21]

In efforts to explore such fundamental questions, the water-soluble Chl-binding protein (WSCP) of higher plants (Figure 1) has emerged as a remarkably tunable model system whose properties can be controlled through site-directed mutagenesis.[22−26] Mutagenesis studies on WSCP have been used to explore the structural basis of pigment-binding selectivity,[27] control over electronic coupling, and the local tuning of both local electronic and vibrational transition frequencies.[23,24] To date, however, little effort has been directed at understanding the role of protein structure in large-scale tuning of vibronic interactions, in either WSCP or other model systems. The manipulation of such parameters using site-directed mutagenesis should offer a promising route to testing fundamental theories about energy transfer in photosynthetic systems by tuning the system through different energy-transport regimes.

Received: June 19, 2024
Revised: August 29, 2024
Accepted: August 30, 2024
Published: September 9, 2024

https://doi.org/10.1021/acs.jpclett.4c01826
J. Phys. Chem. Lett. 2024, 15, 9456−9465

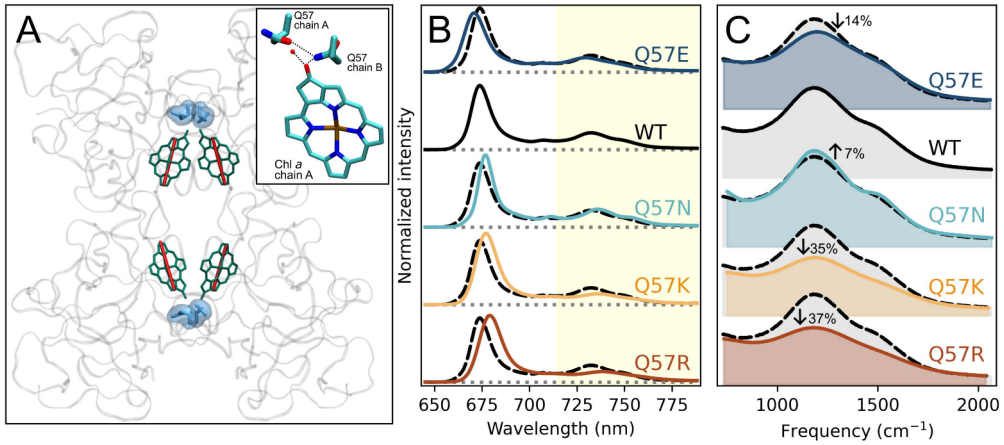

Figure 1. Structure and spectral properties of Chl *a* complexes with WT and Q57 mutants of LvWSCP. (A) Two pairs of strongly coupled Chls in LvWSCP (PDB entry 2DRE). The Chl structure is simplified for clarity. Transition dipole moments of Chls are shown in red. The mutation region is highlighted in blue. Inset: interactions in the vicinity of the 13^1-carbonyl group of Chl *a*. (B) 77 K fluorescence spectra of the Chl *a* complex with LvWSCPs. WT LvWSCP spectrum is plotted (in dashed black) alongside each LvWSCP mutant. The VSB is highlighted in yellow; all spectra are normalized to have the same area. The zero lines are shown in dotted gray. (C) Enlarged VSB. All spectra are shifted to have a Q_y peak at 0 cm^{-1}.

In this work, we explore this possibility by examining the vibrational sideband (VSB) structure in a series of Chl complexes with *Lepidium virginicum* (Lv) WSCP mutants using low-temperature fluorescence spectroscopy (Figure 1A). Our experimental data reveals that single-point mutations of the glutamine-57 (Q57) amino acid residue of the protein lead to significant changes in both the electronic and vibrational structure of the pigment−protein complexes (PPCs). Numerical simulations suggest that these changes can be attributed to delocalization-induced line shape changes that can be disrupted by weakened excitonic interactions. Additional experiments with Chl *a*/Chl *b* and Chl *a*/Zn-Chl *b* heterodimers confirm this assignment, demonstrating that the disruption of excitonic delocalization alone (without local structural changes) is sufficient to substantially alter VSB intensities. These observations point to a potentially significant role for modulating VSB intensities as a "control knob" for tuning energy transfer rates in PPCs and molecular aggregates.

Earlier work on Q57 mutants in LvWSCP focused on predicting experimental shifts of the electronic Q_y transition frequency with molecular dynamics and electrostatic simulations.[26] A simple charge density coupling (CDC) model was found to provide a remarkably accurate description of the mutation-induced shifts observed experimentally, suggesting that the charge of the mutated amino acid residue is the key factor in determining the magnitude and direction of the frequency shift. Briefly, due to differences in Chl *a* ground- and excited-state electronic charge density, positive charges in the vicinity of the Q57 site tend to stabilize the excited state and result in a red shift of the Q_y transition. The case is reversed for negatively charged amino acid residues.

As shown in Figure 1, this trend also holds in 77 K fluorescence spectra (frame B), which peak at longer wavelengths for positively charged mutants and shorter wavelengths for the negatively charged mutant. However, low-temperature fluorescence spectra reveal an additional, unexpected trend (frame C): the positively charged R and K mutants exhibit a substantial decrease in VSB intensity (35−37%) compared to the WT protein. This trend does *not* appear to correlate directly with overall side chain charge since the negatively charged Q57E mutant also exhibits a small drop (14%) in sideband intensity.

A plausible explanation for this effect is suggested by recent theoretical work that suggests that electronic delocalization strongly alters vibrational sideband structure in WSCP.[28] The four Chl molecules are arranged in LvWSCP in a "dimer of dimers" configuration, with an ∼27° angle between the Chl plains in each pair.[29] A relatively short center-to-center distance of 7.4 Å between paired Chls[29−31] leads to strong excitonic interactions with earlier reported electronic coupling values in the range of 84 to 100 cm^{-1}.[29,31,32] This electronic coupling results in excitonic delocalization of the Q_y electronic transition across the pigments within each dimer, while the H-aggregate-like binding geometry results in the suppression of the lower exciton band of the dimer.[10] The theoretical analysis of ref 28, however, suggests that, due to the localized character of high-frequency vibrations,[33,34] high-frequency VSB intensities in fluorescence should *not* be affected by such geometric effects, leading to a relative enhancement of the vibrational sideband relative to the (excitonically suppressed) purely electronic transition.

Applied to our experimental data, this suggests that sideband intensities track changes in electronic coupling strength: since the VSB in WT WSCP is excitonically enhanced, any decrease in intermonomer coupling leads to a corresponding decrease in VSB intensity (Figure 1C). Thus, the weakened sideband intensities exhibited by our Q57K and Q57R mutants may be due to a loss of excitonic delocalization (and the associated suppression of the 0−0 electronic transition) rather than any local change in vibronic coupling parameters. This suggestion is supported by the previous observation that experimental circular dichroism (CD) spectra for the K and R mutants show a pronounced loss of signal in the Q_y range, indicating weakened excitonic delocalization.[26] Although the reason for this weakened delocalization is not entirely clear, electrostatic repulsion between the bulky, positively charged Arg and Lys side chains at the dimer interface (leading to larger interpigment distances) could well play a role.

To test more directly whether electronic delocalization indeed controls the vibrational sideband intensity in WSCP, we prepared heterodimeric LvWSCP complexes reconstituted

https://doi.org/10.1021/acs.jpclett.4c01826
J. Phys. Chem. Lett. 2024, 15, 9456−9465

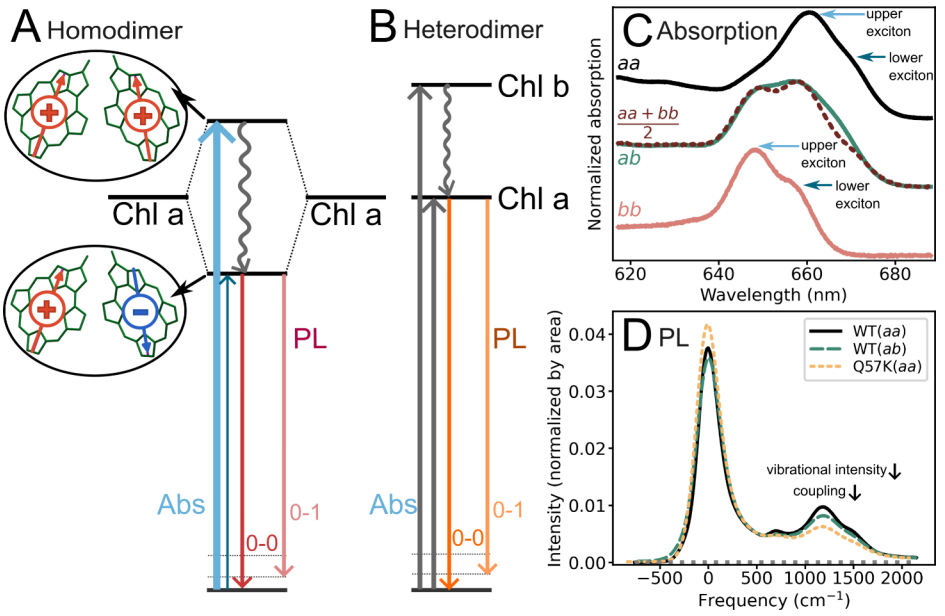

Figure 2. Electronic structure and spectral properties of heterodimeric Chl-LvWSCP complexes. (A) A homodimer of Chl *a* molecules in WT LvWSCP is strongly coupled, leading to the excitonic delocalization between upper and lower excitonic states. (B) (Chl *a*/Chl *b*) pair in WSCP exhibits lower electronic coupling due to significant detuning resulting in localization of excitation energy on Chl *a*. Abs—nonresonant laser excitation at 450 nm, in which excitation of the lower excitonic state in (A) is suppressed due to the dipole−dipole interference; curved arrows, quick relaxation of the system to the lowest electronic excited state; and PL, detected fluorescence. (C) 77 K absorption of homodimeric Chl *a* (*aa*, top), heterodimeric Chl *a*/Chl *b* (*ab*, middle, green), and homodimeric Chl *b* (*bb*, bottom) in WT LvWSCP. The average of *aa* and *bb* is plotted in dashed purple (middle). (D) 77 K PL of Chl-WSCP complexes with different electronic couplings. Black, solid—homodimeric Chl *a* in WT LvWSCP; green, dashed—heterodimeric 1-to-1 (Chl *a*/Chl *b*) in WT LvWSCP; and yellow, dashed—homodimeric Chl *a* in Q57K LvWSCP. The zero line is shown in dotted gray.

with equal concentrations of Chl *a* and Chl *b*. Although we cannot control which binding sites in the protein are occupied by Chl *a* and which sites are occupied by Chl *b*, an overall 50:50 ratio of Chl *a* to Chl *b* in the sample means that (assuming uncorrelated binding) roughly half of Chl *a* molecules will be situated next to a Chl *b* molecule. (Note that under our reconstitution protocol we do not see the large differences in Chl *a* and Chl *b* binding affinity observed by Girr et al. using a different reconstitution procedure.[35]) In such Chl *a*:Chl *b* heterodimers, excitonic delocalization will be largely disrupted due to the 12 nm (262 cm^{-1}) frequency shift between Q_y transition frequencies for Chl *a* and Chl *b*. Although excitonic delocalization is suppressed in these samples, the fluorescence signal at 77 K is still expected to come primarily from Chl *a* since energy will thermalize to the lowest-energy state in the system before being emitted. (Fluorescence is expected from Chl *b* only if all four sites in the complex are occupied by Chl *b*, which, assuming uncorrelated binding of each pigment, should occur with a probability of only $\frac{1}{2^4} \approx 0.0625$.) Thus, the 77 K fluorescence spectra of LvWSCP samples reconstituted with a 50:50 mixture of Chl *a* and Chl *b* are expected to exhibit roughly equal contributions from complexes with and without the influence of excitonic delocalization. If delocalization is, in fact, responsible for modulating VSB intensity, then this effect should be visible in the fluorescence spectra of such complexes even without any change to the local pigment environment.

Frame C of Figure 2 compares 77 K absorption spectra for WT LvWSCP complexes reconstituted with pure Chl *a* (black: labeled "aa"), pure Chl *b* (pink: labeled "bb"), or a 50:50 mixture of Chl *a* and Chl *b* (green: labeled "ab"). For comparison, the dashed purple curve shows the average of the aa and bb spectra. Both aa and bb spectra show clear features corresponding to upper excitons (660.4 and 648.1 nm for aa and bb, respectively) and lower excitons (670 and 657 nm, respectively) of the Chl dimer. These features are still visible in the ab mixture but are much less distinct due to interference from additional bands appearing at 653.4 and 665.8 nm; these new features appear halfway between the upper and lower exciton bands for the dimeric complexes and presumably correspond to the localized absorption transitions of "monomeric" Chl *a* and Chl *b* pigments whose nearest neighbor in the LvWSCP complex is of a different type.

Frame D of Figure 2 plots detector-response-normalized[36] 77 K fluorescence spectra for WT LvWSCP with 50:50 Chl *a*:Chl *b* (dashed green) against spectra for homodimeric WT (black) and Q57K (yellow) reproduced from Figure 1C for comparison. As expected, the disruption of excitonic delocalization in the heterodimer (ab) induces an ∼16% loss in VSB intensity, nearly half of the 35% drop between WT and Q57K Chl *a* homodimeric complexes. This result matches almost exactly what is expected if excitonic delocalization is responsible for modulating the VSB intensity since roughly half of the samples in the 50:50 *a*/*b* mixture will show emission from delocalized Chl *a* homodimers and half from Chl *a*/Chl *b* heterodimers. By contrast, 77 K fluorescence spectra of Q57K LvWSCP Chl *a*/Chl *b* heterodimers showed almost no changes in the VSB intensity compared to homodimeric Q57K LvWSCP (Figure S1 in the Supporting Information). These results strongly support the hypothesis that excitonic delocalization controls the VSB intensity in LvWSCP.

This result can be established more robustly by incorporating into the LvWSCP complex Zn-substituted Chl *b* pigments, whose Q_y transition frequency is blue-shifted by ∼18.9 nm

https://doi.org/10.1021/acs.jpclett.4c01826
J. Phys. Chem. Lett. 2024, 15, 9456−9465

(429 cm^{-1}) from Chl *a* in solution.[37−39] In this case, the Chl *a* and Zn-Chl *b* transitions are sufficiently resolved to allow for direct subtraction of the Zn-Chl *b* fluorescence from the mixed *a*/*b* spectra to extract directly the fluorescence signal from the localized Chl *a* Q_y transition in LvWSCP.

To this end, we prepared heterodimeric Zn-Chl *b*:Chl *a* LvWSCP complexes with a small percentage of Chl *a* included in a predominantly Zn-Chl *b* reconstitution solution. The exact ratio of Chl *a* to Zn-Chl *b* in these complexes is difficult to determine, but an approximate value can be obtained by comparing the relative intensities of the Chl *a* and Zn-Chl *b* features in the fluorescence spectrum. Note that even in the mixed sample, Zn-Chl *b* fluorescence is expected only from homotetrameric complexes in which all four binding sites are occuped by Zn-Chl *b* since any complexes that contain at least one Chl *a* will fluoresce through the Chl *a* transition at 77 K. Thus, Zn-Chl *b* fluorescence line shapes are expected to be identical in both pure Zn-Chl *b* and mixed Chl *a*:Zn-Chl *b* samples.

Frames A (WT) and C (Q57K) of Figure 3 show experimental fluorescence spectra for Chl *a* homodimers

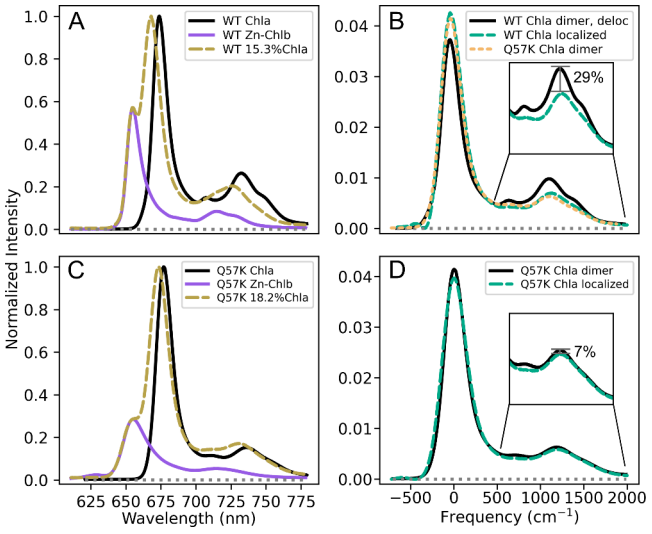

Figure 3. Isolation of the localized Chl *a* fluorescence signal in heterodimeric complexes with Zn-substituted Chl *b*. (A), (C) PL spectra of WT (A) and Q57K (C) LvWSCP reconstituted with Chl *a* (black), Zn-Chl *b* (purple), and a 15% (A) or 19% (C) Chl *a*/Zn-Chl *b* mixture (dashed, yellow). (B), (D) PL spectra of WT (B) and Q57K and (D) LvWSCP reconstituted with dimeric Chl *a* (black) and localized Chl *a* (dashed, green). The zero line is shown in dotted gray. The Chl *a* Q57K PL spectrum is added to frame (B) for comparison (yellow).

(black), Zn-Chl *b* homodimers (purple), and Chl *a*:Zn-Chl *b* mixtures (dashed yellow). The pure Zn-Chl *b* spectra are scaled to match the intensity of the Zn-Chl *b* fluorescence feature in the mixed *a*/*b* samples. In frames A and C, the scaled Zn-Chl *b* spectra comprise 38.5 and 32.5%, respectively, of the total fluorescence signal of the mixed sample. From this ratio, the ratio of Chl *a* to Zn-Chl *b* can be estimated as follows: accounting for an oscillator-strength ratio of 1.7 between Chl *a* and Zn-Chl *b* (see Supporting Information),[40] a fluorescence contribution of 38.5% corresponds to a *homotetrameric* Zn-Chl *b* concentration of 51.5%. As detailed in the Supporting Information, this corresponds to a total Chl *b* fraction of 84.7% in the reconstituted protein or a total Chl *a* fraction of 15.3%. Under these conditions, 90.5% of Chl *a* in the sample is present as a "monomeric" pigment, with only 9.5% present as a dimeric pigment. The same calculation for the Q57K sample indicates a total Chl *a* fraction of 18.2%, implying that 88.2% of Chl *a* fluorescence comes from monomeric pigment and 11.8% comes from dimeric Chl *a* pigments.

Subtracting the scaled pure Zn-Chl *b* fluorescence spectrum from the spectrum of the mixed sample thus produces a fluorescence curve (dashed green lines in frames B and D) that is dominated by the signal from the localized Chl *a* Q_y transition. As expected, the shape of this "localized" Chl *a* fluorescence spectrum closely matches that of the Q57K mutant (dashed yellow line in Frame B), in which excitonic coupling is disrupted. In comparison to WT LvWSCP, the sideband intensity is lower by 29%, close to the 35% loss in intensity seen in the Q57K mutant. (Note that our "localized" spectrum still contains an ∼10% contribution from Chl *a* dimers with elevated sideband intensities.) In the Q57K mixed sample, by contrast, the vibrational sideband intensity in the extracted "localized" spectrum closely matches the sideband intensity for the pure Chl *a* Q57K sample, confirming that excitonic delocalization is almost completely disrupted in the Q57K complex. Note that the close agreement between the Q57K dimer spectrum with the "localized" line shapes for both WT and Q57K confirms that the Q57K mutation does not substantially affect the local vibronic coupling parameters themselves.

These experimental results demonstrate that excitonic delocalization has a substantial impact on VSB intensity in LvWSCP. What remains is to further elucidate the physical mechanism behind this effect and quantify its effect on extracting vibrational Huang−Rhys (HR) factors from the experimental spectra. To this end, we performed numerically exact vibronic mixing simulations of the low-temperature (0 K) fluorescence line shape for Chl *a* dimers in the LvWSCP binding geometry. Briefly, these calculations proceed by building the full Hamiltonian matrix for the coupled vibrational/electronic system,[34,41,42] incorporating 28 Franck−Condon active local vibrations on each pigment. In order to keep the size of the vibronic Hamiltonian tractable, the intensity contribution of each vibronic state was estimated based on HR factors of the contributing vibrational quanta; the states contributing below a given intensity cutoff (10^{-7} for the calculations shown in Figure 4) were truncated. The HR factors for the "monomer" Chl *a* were obtained by starting with the literature values from ref 43 and iteratively adjusting their intensities until a simulated 77 K monomer fluorescence spectrum (using the PigmentHunter app[44]) matches the experimental 77 K spectrum of Q57K, as we take the Q57K spectrum as our experimental reference for a monomer-like system. These "monomer" HR factors were used to represent the spectral density of Chl *a* with a smaller set of vibrations that, together with the vibrations modeling the low-frequency phonon sideband, constituted 28 modes utilized in building the Hamiltonian matrix for the vibronic dimer. Electronic coupling in the dimeric system was set to 130 cm^{-1}, following ref 28. Note that this bare electronic coupling is effectively rescaled by vibronic mixing, which accounts for the smaller coupling value reported in ref 31. The lowest-energy eigenvector of this Hamiltonian is then calculated numerically, which allows for simulation of the 0 K fluorescence spectrum. Further details of the vibronic modeling and the utilized

https://doi.org/10.1021/acs.jpclett.4c01826
J. Phys. Chem. Lett. 2024, 15, 9456−9465

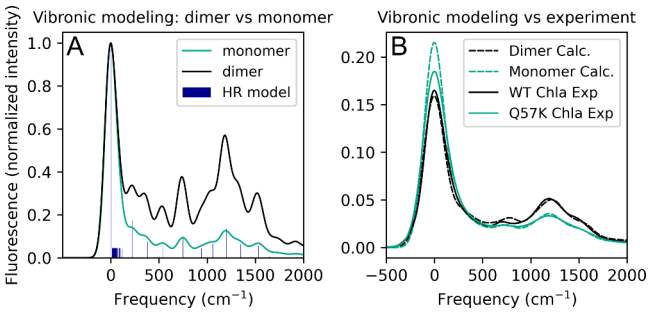

Figure 4. Vibronic modeling of the Chl *a* WSCP complex. (A) Computed 0 K fluorescence spectra of the monomer (cyan) and degenerate dimer (black). HR factors of the vibrational modes utilized for vibronic modeling are shown to scale as blue sticks. The spectra are normalized by the intensity of the 0−0 peak. (B) The modeled monomer spectrum resembles the Q57K mutant spectrum with disrupted excitonic coupling between Chl's (cyan dashed and solid lines). The calculated dimer spectrum incorporates the effect of static disorder and compares with the WT Chl *a* spectrum (dashed and solid black lines). The spectra are normalized by the area. In both frames, the intersite electronic coupling is set to 130 cm^{-1}, with a 30° angle between the transition dipole moments.[28]

vibrational HR factors are provided in the Supporting Information.

Frame A of Figure 4 compares the fluorescence spectrum for a degenerate dimer computed under this method to the fluorescence spectrum of monomeric Chl *a* with the same parameters. Consistent with our experimental data, the high-frequency side of the VSB is strongly enhanced relative to the purely electronic zero-phonon line (ZPL), with the magnitude of the enhancement decreasing gradually with the vibrational frequency.

However, as the vibrational line shape depends sensitively on delocalization across the dimer, the site-energy asymmetry between the two sites, accounting for disorder, is critical to accurately describing the experimental spectrum. To this end, we repeated vibronic calculations for dimers with varying frequency shifts between the site energies of the two monomers to simulate static disorder. Figure 4B compares the full disorder-averaged vibronic spectrum at 0 K from this procedure (dashed lines) with 77 K fluorescence spectra from WT (black) and Q57K (green) LvWSCP. Although some variation in line shape is observed due to the temperature difference between the 77 K experiment and the 0 K simulation (which is difficult to converge at higher temperatures), the intensities of the VSBs in the two cases match quite well. (Note that the slight narrowing of the calculated spectra relative to experiment is expected due to the lower temperature of the simulation; the static disorder parameters

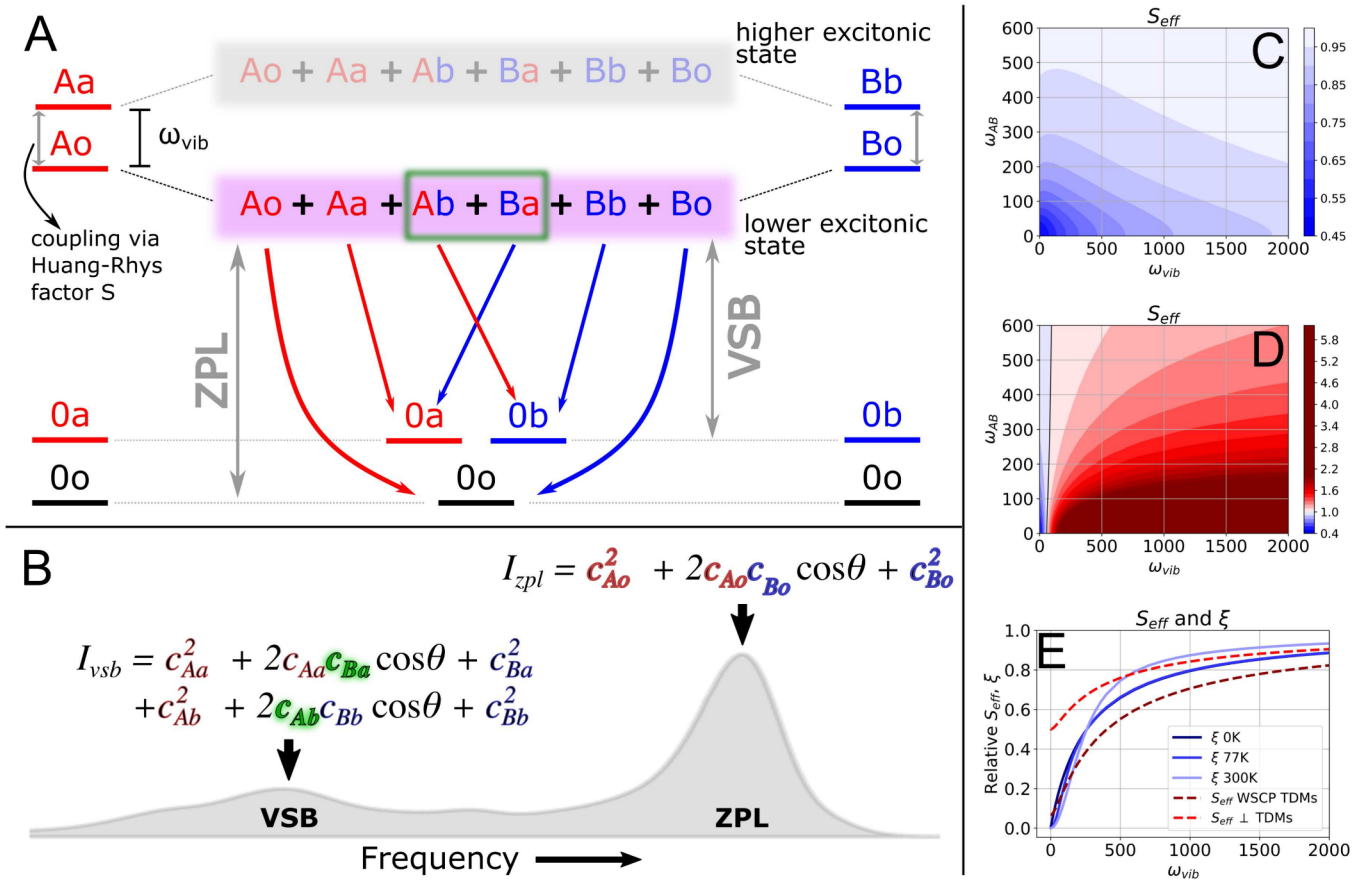

Figure 5. (A) Vibronic mixing schematic for two electronically coupled pigments (A and B) with a single vibrational mode each. (B) Dipole interference effects are always present for the purely electronic ZPL but depend on the presence of cross-terms (c_{Ba} or c_{Ab}) in the VSB. (C) Effective HR factor *S* for fluorescence from a coupled dimer with orthogonal dipoles as a function of the vibrational frequency ω_{vib} or site asymmetry ω_{AB}. (D) Effective HR factor *S* for a coupled dimer with transition dipole vectors matching the WSCP geometry; all other parameters are as in frame C. (E) Comparison of the variation of effective HR values for degenerate coupled dimers (dashed lines) with the variational polaron parameter ξ of ref 45 at various temperatures; all values are rescaled by their $\omega_{vib} \rightarrow \infty$ limit to produce variation between 0 and 1.

https://doi.org/10.1021/acs.jpclett.4c01826
J. Phys. Chem. Lett. 2024, 15, 9456−9465

are set so that the calculated 77 K monomer spectrum matches the 77 K experiment, as described in the Supporting Information.) Although higher-temperature simulations would be required to quantitatively describe the experimental spectra, the present results establish clearly that electronic coupling effects alone (without additional local changes) are sufficient to describe the observed experimental changes in sideband intensity.

To flesh out the physical origins of this effect more fully, Figure 5 schematically outlines the energetic structure of a system of two pigments (denoted A and B) that each couple internally to a single vibrational coordinate (per pigment) and are electronically coupled to each other. The ladder of states on the left and right sides of the diagram represents the energy states of the isolated pigments, with upper-case characters representing electronic excitation and lower-case characters representing vibrational excitations. Thus, "0o" refers to the overall ground state, while "0a" refers to a single vibrational excitation on pigment A, "Ao" refers to purely electronic excitation of pigment A, and "Aa" refers to a mixed vibronic excited state. States "0b", "Bo", and "Bb" represent the equivalent excitations on pigment B.

Note that in what follows we use the ground-state vibrational basis to describe all vibrational excitations; i.e., the states Aa and 0a have the same vibrational wave function. Because the vibrational potential energy surfaces in the electronic ground and excited states are typically shifted relative to each other, states Aa and Ao (and likewise Bb and Bo) are not true eigenstates even for the individual monomer Hamiltonians. Thus, even for the isolated pigments, the ground vibrational wave function of the electronic excited state is a mixture of the Ao and Aa states, which are coupled by a term proportional to the square root of the Huang–Rhys factor S.[34] (In dimensionless coordinates, S represents the displacement between ground- and excited-state vibrational potentials.) It is this "mixing in" of the Aa excitation into the lowest-energy vibrational wave function of the electronic excited state that leads to VSBs in low-temperature fluorescence, since it produces allowed transitions to the 0a vibrational excitation in the electronic ground state.

If we were describing only a single pigment, then it would be most convenient to use two different vibrational basis sets for dynamics in the electronic ground and excited states since there are well-defined vibrational eigenstates for both cases. For the excited states of an excitonically coupled system, however, no corresponding "natural" basis exists. When pigment A is electronically excited, it would be most convenient to use an excited-state vibrational basis for modes localized on pigment A and a ground-state vibrational basis for modes localized on pigment B. However, when pigment B is electronically excited, just the opposite is true: the most convenient choice would be the ground-state basis for A vibrations and the excited-state basis for B vibrations. Because the true system eigenstates are, in general, a superposition of A and B excitations, no single vibrational basis is entirely satisfactory. (The variational polaron transformation, discussed briefly in the conclusion, offers one approach to constructing an optimized but approximate vibrational basis for such systems.[45]) It is for this reason that, throughout our discussion, we use the vibrational basis of the ground electronic state to describe all vibrational excitations.

In the presence of electronic coupling, the picture is complicated by two effects. First, we must consider mixed-character states such as Ab and Ba, where one pigment is electronically excited and the *other* pigment is vibrationally excited. In the absence of electronic coupling, these states are decoupled from the other electronic excited states and thus play no role in electronic spectroscopy. But when both electronic and vibronic interactions are present, they can play an important role in spectroscopy, as we will see in a moment. Second, we must allow coupling between all electronic excited states with common vibrational indices; thus Ao couples to Bo, Aa couples to Ba, and Ab couples to Bb. Note that there is no direct coupling between states with simultaneously different electronic and vibrational indices (e.g., Aa does not directly couple to either Bo or Bb). Nonetheless, the combination of electronic and vibronic coupling is sufficient to allow all six states (Ao, Aa, Ab, Ba, Bb, and Bo) to mix via indirect couplings so that the lowest-energy eigenstate of the electronically excited manifold is, in general, a complicated superposition

$$|\psi_0\rangle = \sum_{\nu} c_{A\nu}|A\nu\rangle + \sum_{\nu} c_{B\nu}|B\nu\rangle \tag{1}$$

where the vibrational index ν takes on the values o, a, and b. It is this complicated eigenstate that is calculated directly in the numerical simulations of Figure 4, except with a larger number of vibrational modes and excitations allowed on each pigment.

With this introduction, we can offer an intuitive explanation for the vibrational localization previously reported in numerical simulations.[28,33,34] Briefly, under the coupling scheme outlined in Figure 5A, the relative contribution of the mixed excitation states Ab and Ba to the fluorescence spectrum depends strongly on the frequency ω_{vib} of the vibration. For low-frequency modes, where all six states are not far from resonance with one another, the Ab and Ba mixed states appear in the fluorescent eigenstate with coefficients comparable to those of monomeric Aa and Bb excitations so that vibrational motion in the electronic excited state is truly delocalized across both sites. With increasing vibrational frequency, however, the Ab and Ba coefficients decrease rapidly so that high-frequency vibrational dynamics in the electronic excited state remain effectively localized to individual monomers even when the 0–0 band is delocalized. This phenomenon has previously been discussed in terms of the dynamic localization of the excitonic wave function,[33,34] although it should be noted that, in our simulations, both static displacements (e.g., the large energy gap between high-frequency states and the delocalized 0–0 transition) and dynamic effects (e.g., the "self-bath" effect from other vibrations[34]) play a role in localizing the high-frequency modes.

This localization of high-frequency vibrations has two effects on the low-temperature fluorescence spectrum. First, it eliminates for high-frequency vibrations the "$1/N$" scaling that, in excitonically delocalized systems, tends to decrease the apparent vibronic coupling strength.[46,47] Intuitively, this effect can be understood as follows: if an electronic excited state is excitonically delocalized across N sites, then the local vibrations of each site on average "feel" the excitation for only $1/N$ of the time. The *average* potential energy surfaces upon which the local vibrations move are thus shifted by only $1/N$ of the displacement under monomeric excitation, leading to an N-fold lower effective vibronic coupling strength. Importantly, this effect depends only on the overall delocalization length, not on the relative geometries of the

https://doi.org/10.1021/acs.jpclett.4c01826
J. Phys. Chem. Lett. 2024, 15, 9456–9465

monomers; thus (given the same intermonomer coupling strength) H- and J-aggregates, for example, are affected similarly. As demonstrated numerically in ref 34, dynamic localization of high-frequency vibrations eliminates this "$1/N$" scaling, with high-frequency modes behaving similarly to individual monomer excitations.

In contrast to this "$1/N$" effect, relative pigment geometry plays a critical role in a second spectroscopic feature that depends sensitively on vibrational localization. In a dimeric system such as WSCP, the fluorescence oscillator strength depends strongly on the relative orientation of the individual pigment transition dipoles and on the relative phase of their oscillations in the fluorescent state. If the monomer dipoles are parallel, for example, in-phase oscillation leads to a "bright" state and out-of-phase oscillation leads to a "dark" state with partially forbidden optical transitions. Because the WSCP dimer features nearly parallel transition dipoles and positive intersite coupling (similar to an H-aggregate), its lowest-energy electronic excited state falls into the latter category, as evidenced by the relative weakness of the lower exciton bands in Figure 2.

To be explicit, the transition strength for fluorescence from the lowest-energy excited eigenstate $|\psi_0\rangle$ to the state 0ν is given by the squared dipole matrix element[34]

$$I_\nu = \| \langle 0\nu | \hat{\boldsymbol{\mu}} | \psi_0 \rangle_{\text{emit}} \|^2 \tag{2}$$

where

$$\hat{\boldsymbol{\mu}} = \boldsymbol{\mu}_A |A\rangle\langle 0| + \boldsymbol{\mu}_B |B\rangle\langle 0| + \text{h.c.} \tag{3}$$

is the electronic dipole moment operator, with "h.c." representing the Hermitian conjugate. Here $\boldsymbol{\mu}_A$ and $\boldsymbol{\mu}_B$ represent the local transition dipole vectors for the two sites. Expanding eq 2 under eq 1 and setting for simplicity $\|\boldsymbol{\mu}_A\|^2 = \|\boldsymbol{\mu}_B\|^2 = 1$ gives for the intensity of the ZPL

$$I_{\text{ZPL}} = {c_{Ao}}^2 + 2c_{Ao}c_{Bo}\cos\theta + {c_{Bo}}^2 \tag{4}$$

and for the VSB

$$I_{\text{VSB}} = {c_{Aa}}^2 + 2c_{Aa}c_{Ba}\cos\theta + {c_{Ba}}^2 + {c_{Ab}}^2 + 2c_{Ab}c_{Bb}\cos\theta + {c_{Bb}}^2 \tag{5}$$

where θ is the angle between the pigment transition dipole moments.

The ${c_{A\nu}}^2$ terms in eqs 4 and 5 represent emission due strictly to excited-state population on pigment A, while the ${c_{B\nu}}^2$ terms represent emission from excited-state population on pigment B; all of these terms are independent of the pigment orientation.

Geometry-dependent effects in eqs 4 and 5 originate from the cross terms, which depend on the angle θ between the pigment transition dipole moments. Importantly, these terms involve *only* coefficients with the same vibrational character (e.g., $c_{Ao}c_{Bo}$, $c_{Aa}c_{Ba}$, or $c_{Ab}c_{Bb}$). Because the electronic-dipole selection rules only allow transitions in which the vibrational index remains unchanged, interference terms do *not* occur involving, for example, coefficient pairs with mixed vibrational indices (i.e., $c_{Aa}c_{Bb}$) even if the vibrational frequencies of the two monomers are identical. As a result, orientation-dependent effects in the VSB must *always* involve one of the two cross-terms c_{Ab} and c_{Ba} (Figure 5B).

When ω_{vib} is small so that the cross-term coefficients c_{Ab} and c_{Ba} are large, the VSB will exhibit the same orientation dependence as the purely electronic ZPL. For high-frequency vibrations, in contrast, c_{Ab} and c_{Ba} tend to be close to zero, and the mechanism for the dipole-orientation dependence in the VSB is lost. In this case, high-frequency vibrations take the same absolute fluorescence intensity as the corresponding transitions in the isolated monomers (i.e., without the influence of either "$1/N$" scaling or orientation dependence due to dipole−dipole interference).

Our numerical simulations reveal that both effects are at work in the WSCP fluorescence spectra. VSB intensities are suppressed near the 0−0 line as a result of both the $1/N$ scaling and geometric suppression of the transition. In contrast, both effects are absent in the high-frequency region, leading to a relative enhancement of the VSB relative to the 0−0 transition. In the intermediate regime, there is a crossover between the two limits, with intensities partially suppressed by $1/N$ scaling and partially enhanced (relative to the ZPL) due to geometric effects. To draw out these trends more clearly, Figure 5C,D plots the "apparent" VSB factor (as judged by the relative intensity of the vibrational peak and ZPL) for a single vibrational transition with frequency ω_{vib} (horizontal axis) whose true VSB factor is $S = 1$ in a dimeric system with 130 cm^{-1} electronic coupling and varying asymmetry $\omega_{AB} = \omega_A - \omega_B$ between the site energies of the two monomers. Frame C corresponds to orthogonal transition dipole moments, where $\cos\theta = 0$ and only $1/N$ scaling contributes to the modulation of VSB intensity. In this case, the true and apparent VSB factors coincide either when V_{AB} is small (so that excitonic delocalization is suppressed) or when ω_{AB} is large (so that the vibrations remain localized). Frame D shows the same calculation when the relative geometry of the monomers matches the dipole orientation in the WSCP complex. In this case, the true and apparent HR factors coincide only in a narrow band (solid black line) along the vertical axis, although the width of this region increases with an increase in the asymmetry ω_{AB} between the sites. When ω_{vib} is very low, excitonic delocalization effects dominate, and the apparent VSB factor is smaller than the true value. When ω_{vib} is large, vibrational localization and geometric effects dominate, producing elevated apparent HR factors.

Real experimental spectra, of course, will be a composite of spectra with a variety of apparent HR factors, determined by the variation in site asymmetries ω_{AB} due to static disorder. In general, disorder is expected to lower the overall variation in VSB intensity, as reflected in the difference between frames A and B of Figure 4. However, to the extent that excitonic delocalization is present in experimental systems, some knowledge of both the delocalization length and the relative geometries of pigments contributing to the fluorescent state will be necessary to extract accurate HR factors from experimental spectra. For orthogonal transition dipoles, only $1/N$ effects are expected to be significant, as discussed recently based on numerical simulations.[34] Accurately accounting for such excitonic effects will also be critical in comparing experimental spectra with spectral densities extracted from atomistic simulations.[48−51]

Finally, we note that the behavior we describe here is in excellent qualitative agreement with recent theoretical predictions based on the variational polaron transformation, in which optical spectra are calculated as a function of a transformation parameter ξ that represents a partial shift of the vibrational basis in the electronic excited state.[45] In close parallel to our observations here, the optimal value of parameter ξ varies for low- and high-frequency vibrations,

https://doi.org/10.1021/acs.jpclett.4c01826
J. Phys. Chem. Lett. 2024, 15, 9456−9465

with low-frequency vibrations experiencing excitonic delocalization (corresponding to $\xi = 0$) and high-frequency vibrations acting as incoherent excitations on each monomer (corresponding to $\xi = \lambda$, where λ is the reorganization energy). For comparison to our numerical results, Figure 5E plots as a function of ω_{vib} the scaling parameter ξ of ref 45 for a degenerate dimer at three different temperatures, alongside our calculated values of S_{eff} from frames C and D. All values are normalized by their high-frequency limits to appear in the range of 0 to 1. Qualitatively, the value of the variational parameter ξ closely tracks the scaling of our S_{eff} values as a function of frequency, suggesting that (although the theory of ref 45 is restricted to fully symmetric, single-mode systems) the variational polaron transform may offer a fruitful approach toward the efficient theoretical description of these effects in experimental systems.

In closing, we note that the interplay that we observe here between excitonic delocalization and vibrational localization is expected to have a considerable impact on energy transfer rates in both PPCs and molecular aggregates. Under both incoherent Förster resonance energy transfer (FRET) and coherent multichromophore FRET (MC-FRET), energy transfer rates are directly proportional to absorption and fluorescence overlap integrals, making the overall energy transfer rate quite sensitive to changes in fluorescence line shape and hence to any enhancement or suppression of VSB intensity. Moreover, since the Chl VSB is dominated by modes with frequencies much larger than the thermal energy $k_BT \approx 210\ cm^{-1}$ available at room temperature, this interplay between excitonic delocalization and vibrational localization is expected to be robust under a wide range of ambient conditions. In future work, it will be of great interest to explore directly the impact of these effects on energy transfer rates and efficiencies in the diverse family of PPCs that governs photosynthetic light harvesting.

■ ASSOCIATED CONTENT

Supporting Information

The Supporting Information is available free of charge at https://pubs.acs.org/doi/10.1021/acs.jpclett.4c01826.

Details on sample preparation, Zn-Chl *b* synthesis, spectroscopic measurements, absorption and fluorescence spectra of Q57K WSCP reconstituted with a Chl *a*/Chl *b* mixture, PL contributions in heterodimeric WSCP complexes with Chl *a*/(Zn-)Chl *b*, elucidation of dipole strength of Zn-Chl *b*, estimation of the Zn-Chl *b* concentration in acetone, disorder averaged line shape calculations, fitting of Huang−Rhys factors, and vibronic modeling (PDF)

■ AUTHOR INFORMATION

Corresponding Author

Mike Reppert − *Department of Chemistry, Purdue University, West Lafayette, Indiana 47907, United States;* orcid.org/0000-0002-7390-3652; Email: reppertm@purdue.edu

Authors

Galina Grechishnikova − *Department of Chemistry, Purdue University, West Lafayette, Indiana 47907, United States*

Jacob H. Wat − *Department of Chemistry, Purdue University, West Lafayette, Indiana 47907, United States*

Nicolas de Cordoba − *Department of Chemistry, Purdue University, West Lafayette, Indiana 47907, United States*

Ethan Miyake − *Department of Chemistry, Purdue University, West Lafayette, Indiana 47907, United States*

Amala Phadkule − *Department of Chemistry, Purdue University, West Lafayette, Indiana 47907, United States*

Amit Srivastava − *Department of Chemistry, Purdue University, West Lafayette, Indiana 47907, United States*

Sergei Savikhin − *Department of Physics and Astronomy, Purdue University, West Lafayette, Indiana 47907, United States*

Lyudmila Slipchenko − *Department of Chemistry, Purdue University, West Lafayette, Indiana 47907, United States;* orcid.org/0000-0002-0445-2990

Libai Huang − *Department of Chemistry, Purdue University, West Lafayette, Indiana 47907, United States;* orcid.org/0000-0001-9975-3624

Complete contact information is available at: https://pubs.acs.org/10.1021/acs.jpclett.4c01826

Notes

The authors declare no competing financial interest.

■ ACKNOWLEDGMENTS

This research was supported in part by the U.S. Department of Energy, Office of Science, Basic Energy Sciences under award DE-SC0022884 and by startup funding from Purdue University. L.S. acknowledges the support of the National Science Foundation (grant CHE-2102639). S.S. and L.S. are supported by the Department of Energy, Office of Basic Energy Sciences (grant DE-SC0018239). This research was partially supported through computational resources provided by Information Technology at Purdue, West Lafayette, Indiana.

■ REFERENCES

(1) Christensson, N.; Kauffmann, H. F.; Pullerits, T.; Mančal, T. Origin of Long-Lived Coherences in Light-Harvesting Complexes. *J. Phys. Chem. B* **2012**, *116*, 7449−7454.

(2) Tiwari, V.; Peters, W. K.; Jonas, D. M. Electronic resonance with anticorrelated pigment vibrations drives photosynthetic energy transfer outside the adiabatic framework. *Proc. Natl. Acad. Sci. U. S. A.* **2013**, *110*, 1203−1208.

(3) Meneghin, E.; Pedron, D.; Collini, E. Raman and 2D electronic spectroscopies: A fruitful alliance for the investigation of ground and excited state vibrations in chlorophyll a. *Chem. Phys.* **2018**, *514*, 132−140.

(4) Romero, E.; Augulis, R.; Novoderezhkin, V. I.; Ferretti, M.; Thieme, J.; Zigmantas, D.; van Grondelle, R. Quantum coherence in photosynthesis for efficient solar-energy conversion. *Nature Phys.* **2014**, *10*, 676−682.

(5) Jonas, D. M. Vibrational and Nonadiabatic Coherence in 2D Electronic Spectroscopy, the Jahn−Teller Effect, and Energy Transfer. *Annu. Rev. Phys. Chem.* **2018**, *69*, 327−352.

(6) Fuller, F. D.; Pan, J.; Gelzinis, A.; Butkus, V.; Senlik, S. S.; Wilcox, D. E.; Yocum, C. F.; Valkunas, L.; Abramavicius, D.; Ogilvie, J. P. Vibronic coherence in oxygenic photosynthesis. *Nature Chem.* **2014**, *6*, 706−711.

(7) Engel, G. S.; Calhoun, T. R.; Read, E. L.; Ahn, T.-K.; Mančal, T.; Cheng, Y.-C.; Blankenship, R. E.; Fleming, G. R. Evidence for wavelike energy transfer through quantum coherence in photosynthetic systems. *Nature* **2007**, *446*, 782−786.

(8) Calhoun, T. R.; Ginsberg, N. S.; Schlau-Cohen, G. S.; Cheng, Y.-C.; Ballottari, M.; Bassi, R.; Fleming, G. R. Quantum Coherence

Enabled Determination of the Energy Landscape in Light-Harvesting Complex II. *J. Phys. Chem. B* **2009**, *113*, 16291−16295.
(9) Collini, E.; Wong, C. Y.; Wilk, K. E.; Curmi, P. M. G.; Brumer, P.; Scholes, G. D. Coherently wired light-harvesting in photosynthetic marine algae at ambient temperature. *Nature* **2010**, *463*, 644−647.
(10) Hestand, N. J.; Spano, F. C. Expanded Theory of H- and J-Molecular Aggregates: The Effects of Vibronic Coupling and Intermolecular Charge Transfer. *Chem. Rev.* **2018**, *118*, 7069−7163.
(11) Halpin, A.; Johnson, P. J. M.; Tempelaar, R.; Murphy, R. S.; Knoester, J.; Jansen, T. L. C.; Miller, R. J. D. Two-dimensional spectroscopy of a molecular dimer unveils the effects of vibronic coupling on exciton coherences. *Nature Chem.* **2014**, *6*, 196−201.
(12) Förster, T. Zwischenmolekulare Energiewanderung und Fluoreszenz. *Ann. Phys.* **1948**, *437*, 55−75.
(13) Arsenault, E. A.; Yoneda, Y.; Iwai, M.; Niyogi, K. K.; Fleming, G. R. The role of mixed vibronic Qy-Qx states in green light absorption of light-harvesting complex II. *Nat. Commun.* **2020**, *11*, 6011.
(14) Arsenault, E. A.; Yoneda, Y.; Iwai, M.; Niyogi, K. K.; Fleming, G. R. Vibronic mixing enables ultrafast energy flow in light-harvesting complex II. *Nat. Commun.* **2020**, *11*, 1460.
(15) Ferretti, M.; Novoderezhkin, V. I.; Romero, E.; Augulis, R.; Pandit, A.; Zigmantas, D.; Grondelle, R. v. The nature of coherences in the B820 bacteriochlorophyll dimer revealed by two-dimensional electronic spectroscopy. *Phys. Chem. Chem. Phys.* **2014**, *16*, 9930−9939.
(16) Kolli, A.; Nazir, A.; Olaya-Castro, A. Electronic excitation dynamics in multichromophoric systems described via a polaron-representation master equation. *J. Chem. Phys.* **2011**, *135*, 154−112.
(17) Kolli, A.; O'Reilly, E. J.; Scholes, G. D.; Olaya-Castro, A. The fundamental role of quantized vibrations in coherent light harvesting by cryptophyte algae. *J. Chem. Phys.* **2012**, *137*, 174109.
(18) Fassioli, F.; Dinshaw, R.; Arpin, P. C.; Scholes, G. D. Photosynthetic light harvesting: excitons and coherence. *Journal of The Royal Society Interface* **2014**, *11*, 20130901.
(19) Chenu, A.; Christensson, N.; Kauffmann, H. F.; Mančal, T. Enhancement of Vibronic and Ground-State Vibrational Coherences in 2D Spectra of Photosynthetic Complexes. *Sci. Rep.* **2013**, *3*, 2029.
(20) Chenu, A.; Scholes, G. D. Coherence in Energy Transfer and Photosynthesis. *Annu. Rev. Phys. Chem.* **2015**, *66*, 69−96.
(21) Chin, A. W.; Huelga, S. F.; Plenio, M. B. Coherence and decoherence in biological systems: principles of noise-assisted transport and the origin of long-lived coherences. *Philosophical Transactions of the Royal Society A: Mathematical, Physical and Engineering Sciences* **2012**, *370*, 3638−3657.
(22) Renger, G.; Pieper, J.; Theiss, C.; Trostmann, I.; Paulsen, H.; Renger, T.; Eichler, H.; Schmitt, F.-J. Water soluble chlorophyll binding protein of higher plants: A most suitable model system for basic analyses of pigment−pigment and pigment−protein interactions in chlorophyll protein complexes. *Journal of Plant Physiology* **2011**, *168*, 1462−1472.
(23) Bednarczyk, D. D.; Dym, D. O.; Prabahar, D. V.; Peleg, D. Y.; Pike, D. H.; Noy, D. D. Fine Tuning of Chlorophyll Spectra by Protein-Induced Ring Deformation. *Angew. Chem.* **2016**, *55*, 6901−6905.
(24) Lahav, Y.; Noy, D.; Schapiro, I. Spectral tuning of chlorophylls in proteins − electrostatics vs. ring deformation. *Phys. Chem. Chem. Phys.* **2021**, *23*, 6544−6551.
(25) Agostini, A.; Meneghin, E.; Gewehr, L.; Pedron, D.; Palm, D. M.; Carbonera, D.; Paulsen, H.; Jaenicke, E.; Collini, E. How water-mediated hydrogen bonds affect chlorophyll a/b selectivity in Water-Soluble Chlorophyll Protein. *Sci. Rep.* **2019**, *9*, 18255.
(26) Srivastava, A.; Ahad, S.; Wat, J. H.; Reppert, M. Accurate prediction of mutation-induced frequency shifts in chlorophyll proteins with a simple electrostatic model. *J. Chem. Phys.* **2021**, *155*, 151102.
(27) Palm, D. M.; Agostini, A.; Pohland, A.-C.; Werwie, M.; Jaenicke, E.; Paulsen, H. Stability of Water-Soluble Chlorophyll Protein (WSCP) Depends on Phytyl Conformation. *ACS Omega* **2019**, *4*, 7971−7979.
(28) Friedl, C.; Fedorov, D. G.; Renger, T. Towards a quantitative description of excitonic couplings in photosynthetic pigment−protein complexes: quantum chemistry driven multiscale approaches. *Phys. Chem. Chem. Phys.* **2022**, *24*, 5014−5038.
(29) Horigome, D.; Satoh, H.; Itoh, N.; Mitsunaga, K.; Oonishi, I.; Nakagawa, A.; Uchida, A. Structural Mechanism and Photoprotective Function of Water-soluble Chlorophyll-binding Protein*. *J. Biol. Chem.* **2007**, *282*, 6525−6531.
(30) Hughes, J. L.; Razeghifard, R.; Logue, M.; Oakley, A.; Wydrzynski, T.; Krausz, E. Magneto-Optic Spectroscopy of a Protein Tetramer Binding Two Exciton-Coupled Chlorophylls. *J. Am. Chem. Soc.* **2006**, *128*, 3649−3658.
(31) Renger, T.; Trostmann, I.; Theiss, C.; Madjet, M. E.; Richter, M.; Paulsen, H.; Eichler, H. J.; Knorr, A.; Renger, G. Refinement of a Structural Model of a Pigment-Protein Complex by Accurate Optical Line Shape Theory and Experiments. *J. Phys. Chem. B* **2007**, *111*, 10487−10501.
(32) Pieper, J.; Rätsep, M.; Trostmann, I.; Schmitt, F.-J.; Theiss, C.; Paulsen, H.; Eichler, H.; Freiberg, A.; Renger, G. Excitonic Energy Level Structure and Pigment-Protein Interactions in the Recombinant Water-Soluble Chlorophyll Protein. II. Spectral Hole-Burning Experiments. *J. Phys. Chem. B* **2011**, *115*, 4053−4065.
(33) Renger, T.; Madjet, M.; Knorr, A.; Müh, F. How the molecular structure determines the flow of excitation energy in plant light-harvesting complex II. *Journal of Plant Physiology* **2011**, *168*, 1497−1509.
(34) Reppert, M. Delocalization Effects in Chlorophyll Fluorescence: Nonperturbative Line Shape Analysis of a Vibronically Coupled Dimer. *J. Phys. Chem. B* **2020**, *124*, 10024−10033.
(35) Girr, P.; Kilper, J.; Pohland, A.-C.; Paulsen, H. The pigment binding behaviour of water-soluble chlorophyll protein (WSCP). *Photochem. Photobiol. Sci.* **2020**, *19*, 695−712.
(36) Gaigalas, A. K.; Wang, L.; He, H.-J.; DeRose, P. Procedures for Wavelength Calibration and Spectral Response Correction of CCD Array Spectrometers. *Journal of Research of NIST* **2009**, *114*, 215−228.
(37) Jones, I. D.; White, R. C.; Gibbs, E.; Denard, C. D. Absorption spectra of copper and zinc complexes of pheophytins and pheophorbides. *J. Agric. Food Chem.* **1968**, *16*, 80−83.
(38) Cogdell, R.; Howard, T.; Isaacs, N.; McLuskey, K.; Gardiner, A. Structural factors which control the position of the Qy absorption band of bacteriochlorophyll a in purple bacterial antenna complexes. *Photosynthesis Research* **2002**, *74*, 135−141.
(39) Orzeł, Ł.; Waś, J.; Kania, A.; Susz, A.; Rutkowska-Zbik, D.; Staroń, J.; Witko, M.; Stochel, G.; Fiedor, L. Factors controlling the reactivity of divalent metal ions towards pheophytin a. *JBIC Journal of Biological Inorganic Chemistry* **2017**, *22*, 941−952.
(40) Knox, R. S.; Spring, B. Q. Dipole Strengths in the Chlorophylls. *Photochem. Photobiol.* **2003**, *77*, 497−501.
(41) Witkowski, A.; Moffitt, W. Electronic Spectra of Dimers: Derivation of the Fundamental Vibronic Equation. *J. Chem. Phys.* **1960**, *33*, 872−875.
(42) Nebgen, B.; Emmert, F. L.; Slipchenko, L. V. Vibronic coupling in asymmetric bichromophores: Theory and application to diphenylmethane. *J. Chem. Phys.* **2012**, *137*, 084112.
(43) Pieper, J.; Rätsep, M.; Trostmann, I.; Paulsen, H.; Renger, G.; Freiberg, A. Excitonic Energy Level Structure and Pigment-Protein Interactions in the Recombinant Water-Soluble Chlorophyll Protein. I. Difference Fluorescence Line-Narrowing. *J. Phys. Chem. B* **2011**, *115*, 4042−4052.
(44) Ahad, S.; Lin, C.; Reppert, M. PigmentHunter: A point-and-click application for automated chlorophyll-protein simulations. *J. Chem. Phys.* **2024**, *160*, 154111.
(45) Bloemsma, E.; Silvis, M.; Stradomska, A.; Knoester, J. Vibronic effects and destruction of exciton coherence in optical spectra of J-aggregates: A variational polaron transformation approach. *Chem. Phys.* **2016**, *481*, 250−261.

https://doi.org/10.1021/acs.jpclett.4c01826
J. Phys. Chem. Lett. 2024, 15, 9456−9465

(46) Cho, M.; Vaswani, H. M.; Brixner, T.; Stenger, J.; Fleming, G. R. Exciton Analysis in 2D Electronic Spectroscopy. *J. Phys. Chem. B* **2005**, *109*, 10542−10556.
(47) Ma, J.; Cao, J. Förster resonance energy transfer, absorption and emission spectra in multichromophoric systems. I. Full cumulant expansions and system-bath entanglement. *J. Chem. Phys.* **2015**, *142*, 094106.
(48) Rosnik, A. M.; Curutchet, C. Theoretical Characterization of the Spectral Density of the Water-Soluble Chlorophyll-Binding Protein from Combined Quantum Mechanics/Molecular Mechanics Molecular Dynamics Simulations. *J. Chem. Theory Comput.* **2015**, *11*, 5826−5837.
(49) Lee, M. K.; Coker, D. F. Modeling Electronic-Nuclear Interactions for Excitation Energy Transfer Processes in Light-Harvesting Complexes. *J. Phys. Chem. Lett.* **2016**, *7*, 3171−3178.
(50) Segatta, F.; Cupellini, L.; Jurinovich, S.; Mukamel, S.; Dapor, M.; Taioli, S.; Garavelli, M.; Mennucci, B. A Quantum Chemical Interpretation of Two-Dimensional Electronic Spectroscopy of Light-Harvesting Complexes. *J. Am. Chem. Soc.* **2017**, *139*, 7558−7567.
(51) Maity, S.; Kleinekathöfer, U. Recent progress in atomistic modeling of light-harvesting complexes: a mini review. *Photosynthesis Research* **2023**, *156*, 147−162.

https://doi.org/10.1021/acs.jpclett.4c01826
J. Phys. Chem. Lett. 2024, 15, 9456−9465